Experimental Measurement of Methane and Carbon Dioxide Clathrate Hydrate Equilibria in Mesoporous Silica

Ross Anderson, Maria Llamedo, Bahman Tohidi,* and Rod W. Burgass

Centre for Gas Hydrate Research, Institute of Petroleum Engineering, Heriot−Watt University, Edinburgh, EH14 4AS, U.K.

Received: June 19, 2002; In Final Form: February 10, 2003

We present experimental structure-I clathrate hydrate (methane, carbon dioxide, and methane−carbon dioxide) equilibrium and ice-melting data for mesoporous silica glass. In both cases, high capillary pressures result in depressed solid decomposition temperatures (clathrate dissociation and ice melting), as a function of pore diameter. Clathrate dissociation data show a significant improvement over existing literature data, which is attributed to the improved experimental techniques and interpretative methods used. Through application of a melting (or clathrate dissociation) modified Gibbs−Thomson relationship to experimental data, we determine similar values of 32 ± 2, 32 ± 3, and 30 ± 3 mJ/m^2 for ice−water, methane clathrate−water, and carbon dioxide clathrate−water interfacial tensions, respectively. The data are important for the accurate thermodynamic modeling of clathrate systems, particularly with respect to subsea sedimentary environments, and should prove useful in the simulation of potential methane hydrate exploitation and carbon dioxide sequestration schemes.

Introduction

Naturally occurring gas hydrates (or clathrates) in sediments pose a hazard to hydrocarbon production operations,[1] have potential as a strategic energy reserve,[2,3] may provide a carbon dioxide sink through sequestration,[4,5] and have long-term importance, with respect to ocean margin stability, methane release, and global climate change.[2,3] However, the thermodynamics of these complex natural systems are still poorly understood.[6,7] Subsea sediments hosting gas hydrates are characterized by fine-grained silts, muds, and clays, usually with very small mean pore diameters (∼0.1 μm).[6,8] Capillary inhibition of hydrate stability in narrow pores has been previously suggested as a possible explanation for differences between predicted (from bulk data) and actual hydrate stability zones.[6]

Handa and Stupin[9] were the first to measure clathrate inhibition (dissociation at lower temperatures or higher pressures relative to bulk conditions) in mesoporous media, which authors attributed to capillary-pressure-induced depression of the water activity. Since then, experimental results from several studies into the effect of narrow pores on clathrate dissociation conditions in porous media have been published.[10−16] In the majority of these studies, the authors employed the Gibbs−Thomson relationship for clathrate growth in narrow capillaries proposed by Clennell et al.[6] and Henry et al.[7] (or derivations thereof) to correlate experimental data, to calculate clathrate−liquid interfacial energies,[11] or to develop thermodynamic models for the prediction of hydrate equilibria in porous media.[12−16]

Although the volume of experimental data for clathrate equilibria in porous media has grown considerably, and the understanding of such systems has consequently improved, a literature review reveals that opinions differ significantly between workers, in regard to appropriate experimental and interpretative methods for such studies, and that significant errors have been introduced as a result. Principal discrepancies concern the following: experimental heating techniques (step heating versus continuous heating); the interpretation of data, with respect to pore size distribution; and the appropriate Gibbs−Thomson relationship that should be used to describe capillary inhibition of clathrate stability (growth versus dissociation hysteresis conditions). In light of the aforementioned issues, we provide, in a companion paper to this work,[17] a review aimed at clarifying the appropriate experimental and interpretative methods for studies of clathrate equilibria in porous media.

In this work, referring to the companion paper as a basis for our interpretations where necessary, we present new, reliable clathrate equilibrium data for methane, carbon dioxide, and methane−carbon dioxide hydrates in confined pores of mesoporous silica glass. These data are used to determine values for structure-I clathrate−water (here, "water" refers to the liquid water phase, of varying dissolved gas concentration) interfacial tensions through a Gibbs−Thomson relationship that describes the temperature depression of clathrate dissociation conditions in cylindrical pores. To validate the equation employed, we calculate ice−water interfacial tension from experimental ice melting point data (for the same porous silica samples), for comparison with established literature values.

Experimental Equipment and Materials

Two separate sets of experimental apparatus were used to generate the data reported in this work: (1) a simple differential temperature setup, for measurement of the ice melting temperatures, and (2) a high-pressure equilibrium cell for the measurement of clathrate dissociation conditions, and for independent confirmation of the ice melting temperatures as determined by setup 1.

The differential temperature setup, shown in Figure 1, consists of a 5 cm^3 aluminum sample tube with a poly(tetrafluoroethylene) sealing sleeve, a central platinum resistance thermometer

10.1021/jp0263370 CCC: $25.00
Published on Web 03/20/2003

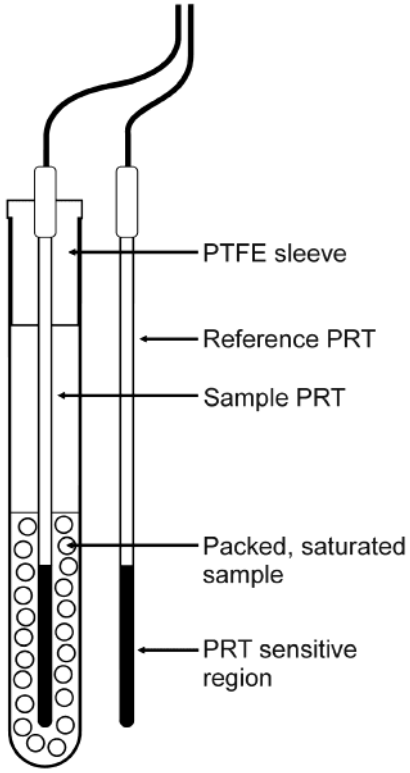

Figure 1. Schematic illustration of the differential temperature apparatus used for ice melting point measurements. Reference PRT measures the bath liquid temperature.

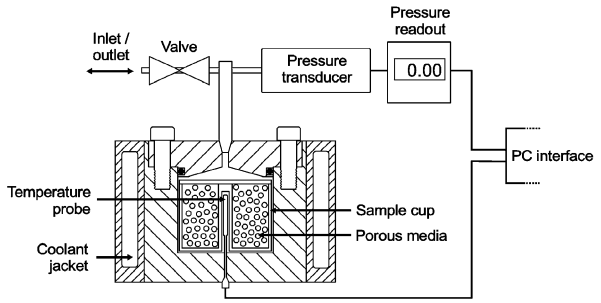

Figure 2. Schematic illustration of the fixed-volume, high-pressure equilibrium cell used for clathrate dissociation point measurements and ice melting point determinations by the isochoric method.

(PRT), and an external reference PRT. During experiments, the aforementioned components are completely immersed within a temperature-controlled bath (253−373 K) that can be kept stable to within ±0.02 K. PRTs were calibrated with an ASL model F250 precision thermometer, and the measurement temperature was calibrated within a precision of ±0.05 K.

The high-pressure setup, shown in Figure 2, consists of an equilibrium cell (maximum pressure of 41.4 MPa), a removable sample cup, a central PRT, an inlet/outlet valve, a Quartzdyne pressure transducer, and a surrounding coolant jacket. The PRT was calibrated with a Prima model 3040 precision thermometer and measures cell temperature within a precision of ±0.01 K. The transducer, when used with a personal computer, can measure pressure within a precision of $\pm 6.9 \times 10^{-6}$ MPa and has a quoted accuracy of ±0.008 MPa for the complete operating range of 0−138 MPa. Cell temperature is controlled by a programmable cryostat (within a range of 253−373 K) and can be kept stable to within ±0.01 K. For both sets of apparatus, the temperature and pressure, where applicable, are continuously monitored and recorded by a computer.

TABLE 1: Porous Silica Glass Specifications, As Determined by NMR Cryoporometry

property	9.2 nm	15.8 nm	30.6 nm
mean pore diameter (nm)	9.2	15.8	30.6
maximum pore diameter (nm)[a]	13.5	23.5	52.5
fraction of porosity (±10%) of mean diameter	0.45	0.68	0.43
specific pore volume (cm^3/g)	0.49	0.87	0.89

[a] Of the detectable porosity (~0.5%).

Double-distilled water was used in all experiments. Methane and carbon dioxide were supplied by Air Products, with both having reported purities of 99.995 mol %. Porous materials were purchased from CPG Inc. USA and consisted of porous silica shards with controlled pore diameters of 37−74 μm. Three samples, with mean pore diameters of 9.2, 15.8, and 30.6 nm, were used for the experiments. Sample pore size distributions were characterized independently by NMR (nuclear magnetic resonance) cryoporometry.[18] Measured specifications are detailed in Table 1.

Experimental Methods: Clathrate Equilibrium Measurements

In a typical test, a porous glass sample is placed in the sample cup, and then distilled water is added to ensure supersaturated conditions (i.e., the volume of water exceeds the pore volume). Prepared samples are then placed in the cell; the cell is cooled (to minimize potential evaporation) and then evacuated. Following evacuation, the appropriate test gas is added through the inlet until the desired initial pressure is reached.

In a typical dissociation point search cycle, cell temperature is first lowered until clathrate formation begins—growth being confirmed by a rapid drop in cell pressure as gas is consumed. Following complete hydrate formation (indicated by stable pressure), the cell temperature is raised in 0.5 K steps, with sufficient time (between 5 and 24 h) being given following each rise to allow the system to reach equilibrium (stable pressure). Cell temperature is continually stepped upward until the initial temperature is reached (which should result in the initial cell pressure conditions) following complete hydrate dissociation. Equilibrium data points, i.e., those where stable pressure has been reached at the end of each temperature step, are used to generate the heating curve for the experiment. This technique, known as step heating, is significantly more reliable and repeatable than conventional continuous-heating methods.[17,19]

Dissociation conditions were determined from the heating-curve data for both mean (d_{mean}) and maximum (d_{max}) pore diameters by the method described in the companion paper to this work.[17] We found heating curves generated using the aforementioned technique to be entirely repeatable, within an error of <0.1 K in the measured mean pore size dissociation conditions for numerous repetitions. As will be shown, the point of final dissociation (at d_{max}) confirms the reliability of mean pore dissociation determinations via the Gibbs−Thomson relationship.

Results: Clathrate Equilibrium Measurements

Experimental clathrate hydrate equilibrium data for methane, carbon dioxide, and methane−carbon dioxide systems in porous silica glass with mean pore diameters of 30.6, 15.8, and 9.2 nm are presented in Tables 2 and 3 and are plotted in Figures 3−5 with comparable literature data where available. A mixed gas composition of 95 mol % methane and 5 mol % carbon dioxide was chosen to simulate the general composition of

TABLE 2: Experimental Methane and Carbon Dioxide Equilibrium Clathrate Dissociation Point Data for Porous Glass Samples (Mean Pore Diameter Data)

9.2 nm		15.8 nm		30.6 nm	
T (K) (±0.1)	*P* (MPa) (±0.008)	*T* (K) (±0.1)	*P* (MPa) (±0.008)	*T* (K) (±0.1)	*P* (MPa) (±0.008)
		Methane			
271.8	3.689	277.8	5.564	280.5	6.405
278.6	7.550	276.9	5.019	283.8	9.170
283.1	12.500	282.9	9.660	287.5	14.065
		285.6	13.307		
		Carbon Dioxide			
272.6	1.931	273.0	1.613	273.1	1.407
274.7	2.544	275.7	2.261	277.9	2.579
270.2	1.448	277.9	3.068	279.8	3.330
		278.2	3.172		

TABLE 3: Experimental Equilibrium Hydrate Dissociation Point Data for 95 mol % Methane−5 mol % Carbon Dioxide Gas Mixture (Mean Pore Diameter Data)

15.8 nm		30.6 nm	
T (K) (±0.1)	*P* (MPa) (±0.008)	*T* (K) (±0.1)	*P* (MPa) (±0.008)
281.3	7.791	280.6	6.205
283.7	10.122	286.5	12.087
285.2	12.231	273.4	2.999

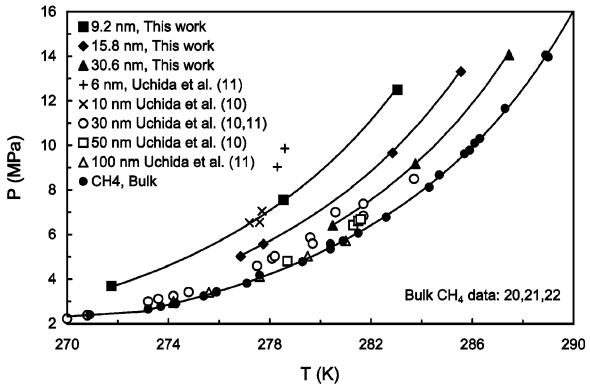

Figure 3. Experimental equilibrium dissociation data (literature and this work) for methane clathrates in mesoporous silica (mean pore diameter data), and under bulk (unconfined) conditions. Solid lines are best-fit curves to data (this work and bulk data only).

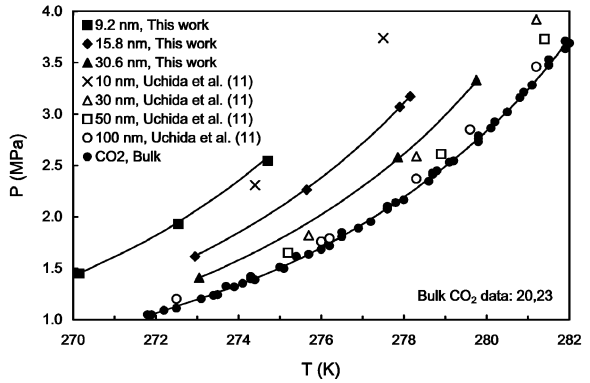

Figure 4. Experimental equilibrium dissociation data (literature and this work) for carbon dioxide (CO_2) clathrates in mesoporous silica (mean pore diameter data), and under bulk (unconfined) conditions. Solid lines are best-fit curves to data (this work and bulk data only).

marine sediment gases. In subsea sediments, bacteriogenically derived gases, although dominated by methane, often are comprised of additional CO_2, with this being reflected in the composition of marine clathrates.

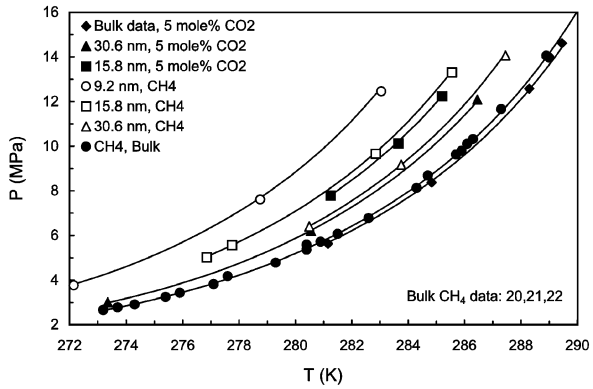

Figure 5. Experimental equilibrium dissociation data (this work) for clathrates formed from a 95 mol % methane−5 mol % carbon dioxide (95 mol % CH_4−5 mol % CO_2) gas mixture in mesoporous silica (mean pore diameter data) and under bulk (unconfined) conditions. Also shown for comparison are pore (this work) and bulk dissociation data (literature data) for methane clathrates. Solid lines are best-fit curves to data.

Results clearly demonstrate the capillary inhibition effect of small-diameter pores on clathrate equilibrium dissociation conditions when compared with bulk (unconfined) systems. The improved quality of data presented here, in comparison with literature data (Figures 3 and 4), advocates the experimental and interpretative methods used.

Experimental Methods: Ice Melting Point Measurements

For validation of the results from the clathrate dissociation point measurements, ice melting temperatures were also measured for porous silica samples. As previously noted, ice melting temperatures were measured by two independent methods: (1) a differential temperature technique and (2) a constant-volume isochoric method. For the differential temperature method, a porous silica sample is first saturated with water (water volume greater than pore volume), and then packed into the aluminum tube (Figure 1) around the PRT to the manufacturer's recommended level. The complete configuration, as shown in Figure 1, is then fully immersed in a temperature-controlled bath. Following supercooling and consequent ice formation inside the porous media, the bath temperature is raised at a constant rate (usually 1 K/min) until the bulk melting point of ice (273.15 K) has been surpassed. During heating, the temperatures of both the sample and reference probes (in the bath) are continuously recorded (once every second).

The theory behind this technique is similar to that for differential scanning calorimetry (DSC), in that the melting of ice is an endothermic reaction, requiring a measurable input of heat. Although actual heat input cannot be accurately determined with the setup described (as it would be in DSC), this process can be quantified in an arbitrary fashion from the temperature difference between the sample and reference probes during ice melting. As the bath temperature is raised, where no ice melting occurs, the sample and reference probe readings will rise comparably in a linear manner. However, during ice melting, the endothermic nature of the reaction causes the sample probe temperature to lag behind the reference probe (bath) temperature as heat is consumed. This lag will ensue until melting is complete, at which point the temperatures of the two probes will converge again. The magnitude of this temperature lag, or deviation (ΔT), at any given sample probe temperature, and the length of time spent at that temperature, are related to the volume of ice melting at that point. This is demonstrated in Figure 6 (inset), where the sample probe temperature is plotted against

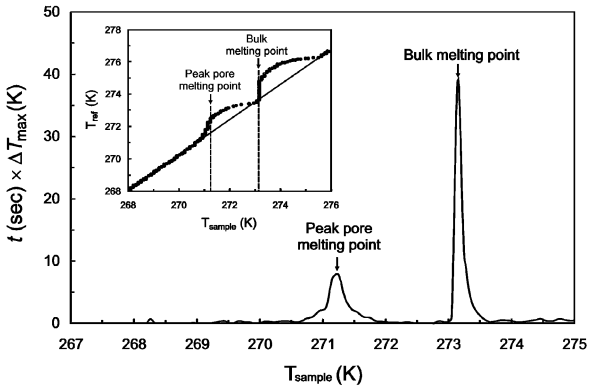

Figure 6. Ice melting point determination by the differential temperature method. Plot shows the sample probe temperature (T_{sample}) against the maximum temperature deviation (ΔT) from the reference probe (T_{ref}), multiplied by the time (t) spent at the sample temperature (in 0.1 K intervals). Inset is a plot of the sample probe temperature against the reference probe temperature during the heating period.

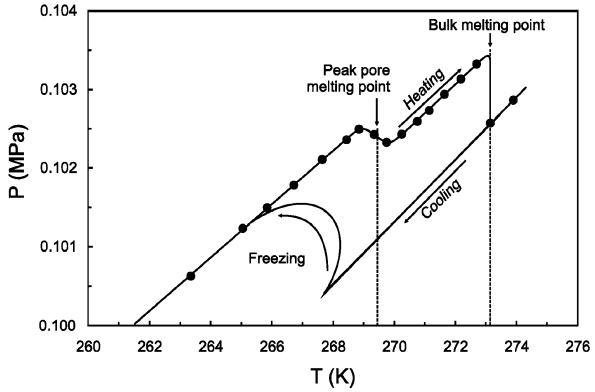

Figure 7. Ice melting point determination using the constant-volume method. Circles represent equilibrium points (5 h per temperature step) for heating. When no melting/freezing occurs, the pressure changes linearly with thermal contraction/expansion. Melting reduces the bulk density, causing a drop in the cell pressure.

the reference probe temperature. Two periods of melting—pore ice (at lower temperatures), and then bulk ice (water outside the pores, beginning at 273.15 K)—are clearly discernible, although the deviation in both cases extends over a wide range of temperatures. To clarify the results for melting peaks, we plot the maximum deviation between the sample and reference probes (ΔT_{max}), multiplied by the time spent (t, in seconds) at any given sample probe temperature. The peaks observed can be considered as an arbitrary function of the volume of ice melting at any given temperature, with the peak pore temperature (269.40 K) and bulk melting points (273.15 K) being clearly observed. This method was found to be repeatable to within ±0.05 K for both pore and bulk melting temperature determinations.

To confirm the accuracy of the aforementioned method independently, we also measured ice melting temperatures for the same porous silica samples by a constant-volume isochoric technique, using the high-pressure cell described (Figure 2). The method is based upon the detection of the bulk density change associated with ice melting. The specific density of ice (~917 kg/m^3) is considerably less than that of liquid water (~1000 kg/m^3); thus, in a constant-volume cell, ice growth or melting will result in a change of system pressure (assuming any change in cell volume is negligible compared to that of water−ice transitions). The advantage of this method is that step heating can be used for the heating cycle, as employed for clathrate dissociation point measurements.

Figure 7 shows a plot of temperature versus pressure for a typical cooling−heating cycle (for the 15.8 nm sample) using this method. When no ice growth or melting occurs, a linear relationship between temperature and pressure (thermal expansion/contraction) is observed. When ice formation occurs on cooling, the bulk density of the system decreases, and a rise in pressure is seen. Upon heating, two periods of melting (as indicated by a drop in pressure) are observed: pore ice, and then bulk ice. Bulk melting occurs at 273.15 K, as would be expected. However, pore melting occurs over a 1.3 K temperature range, between 268.7 and 270 K. This pattern is similar to that observed for clathrate heating curves and can be attributed to melting across the pore size distribution of the sample. The melting point for the mean pore diameter (or diameter of maximum porosity) can be determined, using the same method as that for clathrate data, from the inflection point of the heating curve (peak of melting).

TABLE 4: Ice Melting Temperatures for Porous Silica Samples, As Measured by the Differential Temperature Method and the Constant-Volume Cell Isochoric Method (Atmospheric Pressure)

	T (K) (±0.1)		
method	9.2 nm	15.8 nm	30.6 nm
differential temperature	266.9 267.0	269.5	271.3 271.2
isochoric		269.4	271.3 271.2

The effects of pore size distribution are also reflected in the results from the differential temperature experiments, where a range of pore melting temperatures, with a distinct central peak, can be observed. For all experiments using this method, we found that melting points were within ±0.1 K of those determined by the differential temperature method, confirming the reliability and repeatability of ice melting point data (Table 4).

The Gibbs−Thomson Equation

We employ the Gibbs−Thomson (or Kelvin) relationship proposed by Clennell et al.[6] and Henry et al.,[7] modified here to describe the *melting* conditions (or clathrate dissociation), in accordance with the companion paper to this work.[17] This equation, for cylindrical pores (assumed here), dictates that the temperature depression for the transition from solid to liquid (or from solid to liquid + gas for clathrates) ($\Delta T_{m,pore}$), compared with bulk conditions, $T_{m,bulk}$, can be related to pore diameter, d, by

$$\frac{\Delta T_{m,pore}}{T_{m,bulk}} = \frac{-2\gamma_{sl}\cos\theta}{\rho_s \Delta H_{m,s} d} \quad (1)$$

where ρ_s is the specific density of the solid (ice or clathrate), $\Delta H_{m,s}$ the specific enthalpy of the transition, and cos θ the contact angle between the solid and the pore wall. Assuming an unfrozen liquid layer ($\theta = 0°$, thus cos $\theta = 1$),[6,7] rearrangement of this equation gives

$$\frac{\Delta T_{m,pore}}{T_{m,bulk}} = \left(\frac{-2\gamma_{sl}}{\rho_s \Delta H_{m,s}}\right)\left(\frac{1}{d}\right) \quad (2)$$

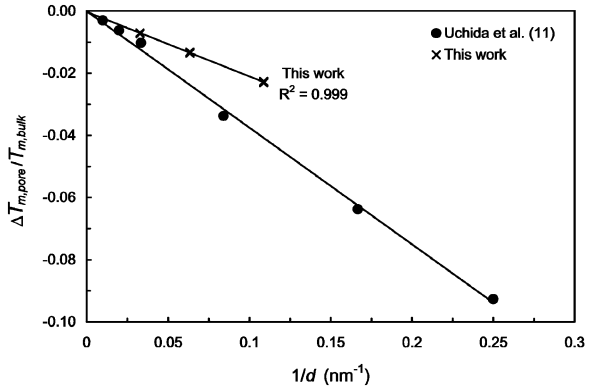

Figure 8. Plot of reciprocal pore diameter ($1/d$) versus $\Delta T_{m,pore}/T_{m,bulk}$ for ice melting in mesoporous silica glass. (From this work and Uchida et al.[11])

Within a limited temperature and pressure range, we can make the assumption that

$$\frac{-2\gamma_{sl}}{\rho_s \Delta H_{m,s}} = \alpha \text{ (constant)} \tag{3}$$

Combination of eqs 2 and 3 gives the following relationship for melting (or dissociation):

$$\frac{\Delta T_{m,pore}}{T_{m,bulk}} = -\alpha\left(\frac{1}{d}\right) \tag{4}$$

When plotted, this relationship should give a trend of slope α, with zero as its origin, because, as pore size becomes increasingly large, the value $1/d$ approaches zero, as does $\Delta T_{m,pore}/T_{m,bulk}$.

At this point, it is important to comment on the presence of an unfrozen layer between the solid phase and the pore walls, as assumed in the equations presented here. It is generally accepted that a narrow unfrozen liquid layer, a few angstroms in thickness, exists between the solid phase and the pore walls for ice and other polar and nonpolar organic solids in confined pores.[24−27] It is necessary to consider the potential control this layer may have on effective pore diameter, i.e., the diameter seen by the solid phase. Pore size distributions for porous silica samples used in this work were determined by NMR cryoporometry,[18] with water (ice) as the test fluid. An unfrozen liquid water layer would be expected to be present between the ice and the silica pore walls during NMR analysis, so measured pore diameters can be considered to be effective pore diameters (true diameter minus the unfrozen layer) for ice. The physical properties of ice and clathrates are similar;[2] therefore, a comparable unfrozen layer thickness can be assumed, meaning the effective pore radii for clathrates should be the same as those for ice. Our calculations are based on this assumption.

Experimental data for ice, methane, carbon dioxide, and methane−carbon dioxide clathrates, and comparable literature data (where available), are plotted with respect to eq 4 in Figures 8−11. Data for the mean pore diameters measured in this work (d_{mean}) give linear fits (origins at zero) with good regression coefficients for all ($r^2 > 0.99$). Data for complete pore hydrate dissociation, at maximum pore diameters (d_{max}), show the same linear relationship, confirming the reliability of experimental and interpretative methods used to generate data. Although scattered, literature data for both methane and carbon dioxide clathrates show a similar trend to the slope of data presented here (Figures 9 and 10). In addition, both sets of data suggest

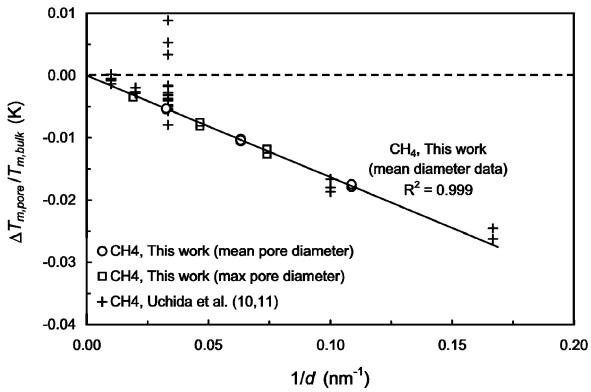

Figure 9. Plot of reciprocal pore diameter ($1/d$) versus $\Delta T_{m,pore}/T_{m,bulk}$ for methane (CH_4) clathrate equilibrium dissociation in mesoporous silica glass (this work and literature data). The linear fit is for mean pore diameter using data generated in this work only.

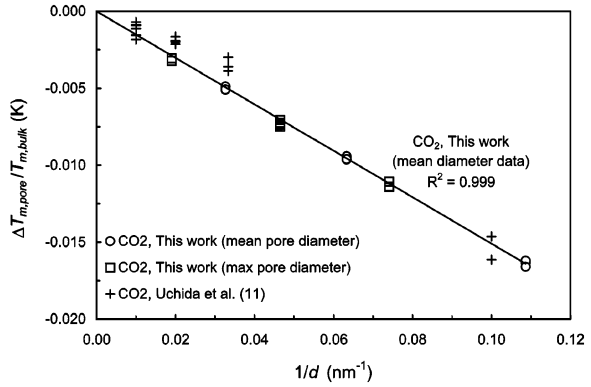

Figure 10. Plot of reciprocal pore diameter ($1/d$) versus $\Delta T_{m,pore}/T_{m,bulk}$ for carbon dioxide (CO_2) clathrate equilibrium dissociation in mesoporous silica glass (this work and literature data). The linear fit is for mean pore diameter data generated in this work only.

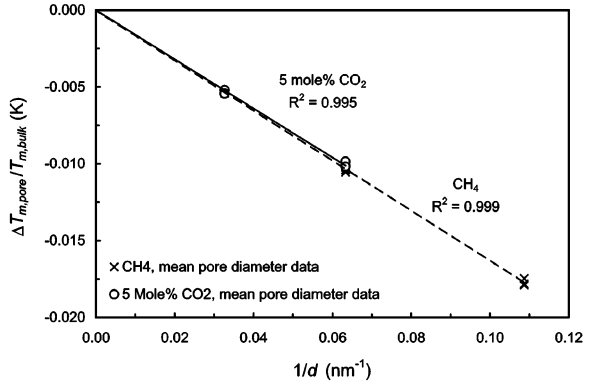

Figure 11. Plot of reciprocal pore diameter ($1/d$) versus $\Delta T_{m,pore}/T_{m,bulk}$ for hydrates formed from a 95 mol % methane−5 mol % carbon dioxide (95 mol % CH_4−5 mol % CO_2) gas mixture in mesoporous silica glass (mean pore diameter data, this work). Data for methane hydrates (mean pore diameter, this work) are shown for comparison. The addition of CO_2 to the gas mixture lowers the slope (solid line), in agreement with data for CO_2 clathrates.

that the slope for carbon dioxide is less than that of methane, as noted by Uchida et al.[11]

For ice, significant deviation between the data generated here and that reported by Uchida et al.[11] is observed, the latter displaying increasingly larger ΔT values with decreasing pore diameter. We propose that this difference in results can be attributed to errors in the methods used by the authors to interpret DSC data. Uchida et al.[11] stated that melting points for ice in pores of mean diameter were determined as the *starting*

TABLE 5: Comparison between Literature Values for Ice−Water Interfacial Tension (γ_{iw}) and That Derived Here (This Work)

method	γ_{iw} (mJ/m^2)	reference(s)
melting/freezing in pores	32 ± 2	this work
	58 ± 12 (29 ± 6)[a]	11
	31 ± 3	29
	29 ± 3	30
	33 ± 1	31
contact angle	33 ± 3	32
crystal growth	32 ± 2	33
shape of grain boundary groove	29 ± 1	34
	44 ± 10	35, 36
growth velocity of dendrites	28	37, 38
morphological instability	25	39

[a] Values recalculated from experimental data for ice melting conditions using eq 1. Original value quoted by the authors is shown in parentheses.

point of melting for each sample. Because of the effects of pore size distribution, the point of first melting will actually represent melting in the smallest pores of the distribution (of detectable porosity), not pores of mean diameter, which those authors attributed to data (the DSC endothermic peak generally corresponds to melting in pores of mean diameter, or diameters of maximum porosity).

Using eq 1, with appropriate density and enthalpy data, the slopes of Figures 8−10 can be used to estimate values for structure-I clathrate−water and ice−water interfacial tensions.

Ice−Water Interfacial Tension

For ice, we employ established values of 6.01 kJ/mol and 917 kg/m^3 for the enthalpy of fusion (melting/freezing) and density (ρ_i), respectively.[28] These values yield an ice−water interfacial tension (γ_{iw}) of 32 ± 2 mJ/m^2—a value closely comparable to the literature values (Table 5). This advocates the experimental methods used to generate data and validates the Gibbs−Thomson relationship employed in solid−liquid interfacial tension calculations (eq 1).

Uchida et al.[11] employed the Gibbs−Thomson equation for *freezing* when calculating ice−water interfacial tension from ice melting data.[17] If data presented by the authors are used to recalculate ice−water interfacial tension, on the basis of eq 1 (essentially doubled), then a value of 58 ± 12 mJ/m^2 is obtained. This value is not within the error of the majority of literature values (Table 5), supporting previous comments concerning the reliability of experimental data.

Clathrate−Water Interfacial Tension

The use of eq 1 to calculate the clathrate−water interfacial tensions requires accurate knowledge of the specific enthalpy of hydrate dissociation ($\Delta H_{h,d}$, or $\Delta H_{m,s}$ in eq 1) and stoichiometric data (water-to-gas ratios) for the calculation of hydrate density. It is important to note that $\Delta H_{h,d}$ is likely to vary with pressure and temperature conditions, as will density, because of variation in the cage occupancy by gas molecules. However, the good linear relationships observed between temperature depression and pore diameter (Figures 9−11) for hydrate data suggest that this variation is not great over the pressure/temperature range studied in this work.

Experimental clathrate $\Delta H_{h,d}$ and stoichiometric data have been principally derived through calorimetric studies of equilibria under bulk conditions. $\Delta H_{h,d}$ values of 53.2−57.7 kJ/mol have been measured for methane hydrates, with hydration ratios generally close to 6:1 (water-to-methane ratio),[40−43] corresponding to average densities of ∼914 kg/m^3.[2] Applying these values to eq 1, from the slope of data in Figure 9, we obtain an average value for methane hydrate−water interfacial tension (γ_{hw}) of 32 ± 3 mJ/m^2 (Table 6). This value is closely comparable with that calculated for the ice−water interfacial energy.

Kang et al.[43] measured the enthalpy of carbon dioxide clathrate dissociation as 65.22 kJ/mol (by DSC). A measured hydration ratio of 7.23:1 gives a clathrate density of 1065 kg/m^3.[2] Using these values, we calculate a carbon dioxide hydrate−water interfacial tension of 30 mJ/m^2 from the slope of data in Figure 10 (Table 6). In accordance with methane hydrate data, we assume a similar error of at least ±3 mJ/m^2. The value 30 ± 3 mJ/m^2 is comparable with, although slightly lower than, those calculated for both methane clathrate−water and ice−water interfacial tensions. This may very well reflect a lower carbon dioxide clathrate−water interfacial energy; however, the lack of data for carbon dioxide clathrate $\Delta H_{h,d}$ means that this cannot be firmly concluded. Ultimately, the estimated value for the carbon dioxide clathrate−water interfacial tension, and that for the methane hydrate−water interfacial tension, would be improved with experimental calorimetric and stoichiometric data for a wide range of temperature/pressure conditions.

The only available literature values (that we are aware of) for methane and carbon dioxide clathrate−water interfacial tensions are those determined by Uchida et al.[11] However, these values were calculated from experimental dissociation data through a Gibbs−Thomson relationship that describes clathrate *growth* in porous media, not dissociation (considerable hysteresis

TABLE 6: Summary of Values for Hydrate−Water Interfacial (γ_{hw}) Tension Calculated Using Eq 1

	$\Delta H_{h,d}$ (kJ/mol)	reference for $\Delta H_{h,d}$ data	ρ_h (kg/m^3)	hydration (water:gas)	γ_{hw} (mJ/m^2)
			Methane		
this work	53.2	40	914	6:1	32 ± 1
	53.3	41	914	6:1	32 ± 1
	54.2	42	914	6:1	33 ± 1
	56.8	43	907	6.4:1	32 ± 1
	57.7	40	914	6:1	35 ± 1
Uchida et al.[11]	54.2[b]	42	914[b]	6:1[b]	34 ± 6 (17 ± 3)[c]
			Carbon Dioxide		
this work	65.2	43	1065	7.23:1	30 ± 1
Uchida et al.[11]	59.9[b]	44	1054[b]	7.3:1[b]	28 ± 6 (14 ± 3)[c]

[a] Values given for "this work" have been calculated from experimental data presented in this paper, on an individual basis for each quoted clathrate dissociation enthalpy ($\Delta H_{h,d}$), hydration ratio, and hydrate density (ρ_h) (from literature experimental data, as referenced). Densities were calculated for appropriate hydration ratios, on the basis of an empty structure-I lattice density of 796 kg/m^3.[2] Errors are experimental errors for each $\Delta H_{h,d}$ and hydrate density (ρ_h) employed. For literature data (Uchida et al.[11]), values are those used by authors. [b] Values as employed by Uchida et al.[11] [c] Values recalculated from experimental data for clathrate dissociation condition, using eq 1. Original value quoted by authors is shown in parentheses.

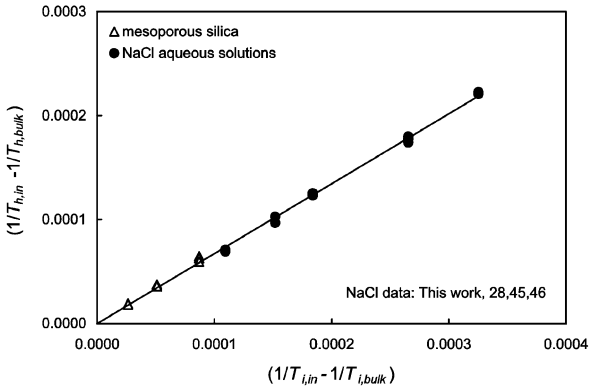

Figure 12. Linear relationship between ice melting and clathrate dissociation temperature depression for capillary (mesoporous silica) and electrolyte (NaCl) inhibition. $T_{h,in}$ and $T_{i,in}$ are the inhibited hydrate dissociation and ice melting temperatures, respectively. $T_{h,bulk}$ and $T_{i,bulk}$ (273.15 K) are the hydrate dissociation and ice melting temperature, respectively, for bulk (uninhibited) conditions. Average measured ice melting temperatures were used for mesoporous silica data.

differentiating these phase transitions).[17] When values are recalculated using eq 1 for appropriate dissociation hysteresis conditions, similar values (within the experimental error of data) to those determined here are observed (Table 6).

Relationship between Capillary Pressure and Water Activity Depression

Considering the similarities between the physical properties of ice and clathrates,[2] it seems reasonable that solid−liquid interfacial tensions for these compounds should be comparable, as has been assumed in previous modeling studies.[6,7,12−16] The similarity of values for interfacial tension suggests that this is not the principal factor controlling the temperature depression of hydrate dissociation and ice melting temperatures in porous media. It has previously been proposed that capillary inhibition is comparable to that resulting from a depression in the water activity, such as that which is caused by thermodynamic inhibitors (e.g., electrolytes and organic inhibitors).[9−11] This proposal can be tested by comparing clathrate dissociation and ice melting temperature depressions for porous media and for electrolyte inhibition (for unconfined conditions), as demonstrated in Figure 12. The observed linear relationship confirms that capillary inhibition closely approximates that resulting from the depression of the activity of water by thermodynamic inhibitors.

With respect to subsea clathrate systems, our results demonstrate that pore size could have a significant effect on hydrate stability in sediments. In fine-grained silts, muds, and clays that host gas hydrates, mean pore diameters of 0.1 μm (100 nm) and smaller are common.[6,8] On the basis of the results presented here, pore sizes of 0.1 μm could inhibit clathrate stability by ∼0.5 K from bulk (unconfined) conditions (for any given pressure), which could be sufficient to shift the base of hydrate stability by tens of meters at low geothermal gradients (based on an average gradient of ∼30 K/km, the shift would be ∼17 m for 0.1 μm pores). However, it is important to note that this information applies to actual clathrate thermodynamic stability—as governed by dissociation conditions—not crystal growth. As discussed in the companion paper,[17] the difference between the clathrate−liquid interface curvatures during growth and dissociation results in considerable hysteresis between these transitions. This hysteresis is such that the conditions under which clathrate growth can occur in a porous medium may be significantly more inhibited than actual thermodynamic stability: the ΔT value for growth is effectively double that for dissociation, based on interface curvatures of $2/r$ and $1/r$, respectively (see companion paper for details). This means that, under appropriate conditions, although clathrate may be theoretically stable within a sediment, hydrate growth may not be possible (as discussed by Clennell et al.[6] and Henry et al.[7]).

Conclusions

Experimental ice melting and methane, carbon dioxide, and methane−carbon dioxide clathrate dissociation conditions for mesoporous silica glass with pore diameters of 9.2, 15.8, and 30.6 nm are reported. As expected, the temperatures for transitions from ice to water, and from clathrate to water + gas, were found to be a strong function of pore diameter. Data show significant improvement on existing literature data and are in good agreement with the linear relationship predicted by the Gibbs−Thomson equation for melting (or dissociation) within cylindrical pores.

Values for the structure-I clathrate−water interfacial energies are conservative estimates, being dependent on available physical property data, although they can be considered to be the most reliable to date. Results could be used in the development and validation of thermodynamic models capable of predicting gas hydrate stability in porous media. The data should also prove useful in the modeling of possible methane exploitation and/or carbon dioxide sequestration schemes.

Acknowledgment. This work was supported by EPSRC (Engineering and Physical Science Research Council) Grant No. GR/M61221 and a SHEFC (Scottish Higher Education Funding Council) Research Development Grant, which are gratefully acknowledged. The authors wish to thank Dr. Kasper Østergaard and Dr. Ben Clennell, for invaluable discussions, and Mr. Jim Pantling, for the manufacture and maintenance of experimental equipment. Thanks are also given to Dr. Beau Webber, University of Kent, for NMR analysis of the porous silica samples.

References and Notes

(1) Milkov, A. V.; Sassen, R.; Novikova, I.; Mikhailov, E. *Trans.−Gulf Coast Assoc. Geol. Soc.* **2000**, *L*, 217.
(2) Sloan, E. D. *Clathrate Hydrates of Natural Gases*, 2nd ed.; Marcel Dekker: New York, 1998.
(3) Kvenvolden, K. A. *Proc. Natl. Acad. Sci. U.S.A.* **1999**, *96*, 3420.
(4) Ohgaki, K.; Takano, K.; Sangawa, H.; Matsubara, T.; Nakano, S. *J. Chem. Eng. Jpn.* **1996**, *29*, 478.
(5) Nakano, S.; Yamamoto, K.; Ohgaki, K. *Proc. Inst. Mech. Eng., Part A* **1998**, *212*, 159.
(6) Clennell, M. B.; Hovland, M.; Booth, J. S.; Henry, P.; Winters, W. J. *J. Geophys. Res. B* **1999**, *104*, 22985.
(7) Henry, P.; Thomas, M.; Clennell, M. B. *J. Geophys. Res. B* **1999**, *104*, 23005.
(8) Griffiths, F. J.; Joshi, R. C. *Geotechnique* **1989**, *39*, 159.
(9) Handa, Y. P.; Stupin, D. *J. Phys. Chem.* **1992**, *96*, 8599.
(10) Uchida, T.; Ebinuma, T.; Ishizaki, T. *J. Phys. Chem. B* **1999**, *103*, 3659.
(11) Uchida, T.; Ebinuma, T.; Takeya, S.; Nagao, J.; Narita, H. *J. Phys. Chem. B* **2002**, *106*, 820.
(12) Wilder, J. W.; Seshradi, K.; Smith, D. H. *J. Phys. Chem. B* **2001**, *105*, 9970.
(13) Seshradi, K.; Wilder, J. W.; Smith, D. H. *J. Phys. Chem. B* **2001**, *105*, 2627.
(14) Smith, D. H.; Wilder, J. W.; Seshradi, K. *AIChE J.* **2002**, *48*, 393.
(15) Smith, D. H.; Wilder, J. W.; Seshradi, K.; Zhang, W. *Proceedings of the 4th International Conference on Gas Hydrates (ICGH4)*, Yokohama, Japan, May 19−23, 2002; p 295.
(16) Zhang, W.; Wilder, J. W.; Smith, D. H. *Proceedings of the 4th International Conference on Gas Hydrates (ICGH4)*, Yokohama, Japan, May 19−23, 2002; p 321.

(17) Anderson, R.; Llamedo, M.; Tohidi, B.; Burgass, R. W. *J. Phys. Chem. B* **2003**, *107*, 3500.
(18) Webber, J. B. W. Characterising Porous Media. Ph.D. Thesis, University of Kent, Canterbury, UK, 2000.
(19) Tohidi, B.; Burgass, R. W.; Danesh, A.; Østergaard, K. K.; Todd, A. C. *Ann. N.Y. Acad. Sci.* **2000**, *912*, 924.
(20) Deaton, W. M.; Frost, E. M. *U.S. Bur. Mines Monogr*. **1946**, *8*, 101.
(21) McLoed, H. O.; Campbell, J. M. *J. Petrol. Technol.* **1961**, *222*, 590.
(22) Jhaveri, J.; Robinson, D. B. *Can. J. Chem. Eng.* **1965**, *43*, 75.
(23) Larson, S. D. Phase Studies Involving the Two-Component Carbon Dioxide−Water System, Involving the Carbon Dioxide Hydrate. Ph.D. Thesis, University of Illinois, Champaign, IL, 1955.
(24) Churaev, N. V.; Bardasov, S. A.; Sobolev, V. D. *Colloids Surf. A* **1993**, *79*, 11.
(25) Ishikiriyama, K.; Todoki, M.; Motomura, K. *J. Colloid Interface Sci*. **1995**, *171*, 92.
(26) Faivre, C.; Bellet, D.; Dolino, G. *Eur. Phys. J. B* **1999**, *7*, 19.
(27) Radhakrishnan, R.; Gubbins, K. E.; Sliwinska-Bartkowiak, M. *J. Chem. Phys.* **2002**, *116*, 1147.
(28) Weast, R. C., Astle, M. J., Beyer, W. H., Eds. *CRC Handbook of Chemistry and Physics*; CRC Press, Inc.: Boca Raton, FL; 1989.
(29) Hillig, W. B. *J. Cryst. Growth* **1998**, *183*, 463.
(30) Enüstün, B. V.; Şentürk, H. S.; Yurdakull, O. *J. Colloid Interface Sci.* **1978**, *65*, 509.
(31) Rennie, G. K.; Clifford, J. *J. Chem. Soc., Faraday Trans.* **1977**, *73*, 680.
(32) Ketcham, W. M.; Hobbs, P. V. *Philos. Mag.* **1969**, *19*, 1161.
(33) Fernandez, R.; Barduhn, A. J. *Desalination* **1967**, *3*, 330.
(34) Hardy, S. C. *Philos. Mag.* **1977**, *35*, 471.
(35) Jones, D. H. R. *Philos. Mag.* **1973**, *27*, 569.
(36) Jones, D. H. R. *J. Mater. Sci.* **1974**, *9*, 1.
(37) Langer, J. S.; Sekerka, R. F.; Fujioka, T. *J. Cryst. Growth* **1978**, *44*, 414.
(38) Furukawa, Y.; Shimada, W. *J. Cryst. Growth* **1993**, *128*, 234.
(39) Coriel, S. R.; Hardy, S. C.; Sekerka, R. F. *J. Cryst. Growth* **1971**, *11*, 53.
(40) Levois, J. S.; Perkins, R.; Martin, R. J.; Kobayashi, R. *Fluid Phase Equilib.* **1990**, *59*, 73.
(41) Reuff, R. M.; Sloan, E. D. *AIChE J.* **1988**, *34*, 1468.
(42) Handa, Y. P. *J. Chem. Thermodyn.* **1986**, *18*, 915.
(43) Kang, S.-P.; Lee, H.; Ryu, B.-J. *J. Chem. Thermodyn.* **2001**, *33*, 513.
(44) Uchida, T.; Hondoh, T.; Mae, S.; Kawabata, J. *In Direct Ocean Disposal of Carbon Dioxide*; Handa, N., Ohsumi, T., Eds.; Terra Science Publishing Co. (TERRAPUB): Tokyo, 1995; p 45.
(45) de Roo, J. L.; Peters, C. J.; Lichtenthaler, R. N.; Diepen, G. A. M. *AIChE J.* **1983**, *29*, 651.
(46) *International Critical Tables of Numerical Data, Physics, Chemistry and Technology*; National Research Council: Washington, DC, 1926−1930; pp 1−7.